Critical currents in bulk superfluid ^{3}He-A

Alexander L. Fetter
Institute of Theoretical Physics, Department of Physics, Stanford University, Stanford, California 94305
(Received 2 February 1981)

The stability of uniform textures in superfluid ^{3}He-A is studied with the phenomenological equations of orbital dynamics. For a fixed applied magnetic field, the texture becomes dynamically unstable at a critical current that depends both on the field $\vec{H}$ and on the angle χ between the flow and the field. In addition, the instability signals a deformation with a finite wave vector (not, in general, parallel to $\hat{l}$) that also depends on H and χ. Beyond threshold, the unstable amplitude does not saturate at some nearby small deformation but instead experiences catastrophic nonlinear growth. Comparison with recent observations suggests other possible experiments.

I. INTRODUCTION

The orbital dynamics of bulk superfluid ^{3}He-A is rich and diverse, for it involves both the external hydrodynamic flow and, through the dipole coupling, the applied magnetic field. Recent theoretical studies[1–4] have concentrated on the particular situation of given flow, in which the system is subjected to an increasing magnetic field parallel to the flow. In this case, the initially uniform texture deforms first into a helical one, which then becomes dynamically unstable with respect to long-wavelength fluctuations at a critical magnetic field. Many other possibilities exist, however, and Paalanen and Osheroff[5] have performed experiments on the complementary situation of a given magnetic field, in which the texture is then subjected to an increasing hydrodynamic flow. For small flow rates, the motion remains frictionless, but dissipation starts to appear at a critical value that signals a significant change in the flow. Related phenomena had been seen earlier by Flint, Mueller, and Adams,[6] including time-dependent shifts in the NMR, presumably indicating persistent motion of the texture.

To help understand these observations, it seemed useful to consider the behavior of bulk superfluid ^{3}He-A in a uniform magnetic field $\vec{H}$ and mass current $\vec{j}$, which need not be parallel. If $\vec{j}=0$, the internal vectors $\hat{l}$ and $\hat{d}$ are parallel and in the plane perpendicular to $\vec{H}$. Nonzero $\vec{j}$ lifts the rotational degeneracy about $\hat{H}$ and orients $\hat{l}$ and $\hat{d}$ in the plane of $\vec{H}$ and $\vec{j}$. Section II studies the static equilibrium for an arbitrary angle χ between $\vec{H}$ and $\vec{j}$, showing that, in general, the uniform texture of $\hat{l}$ and $\hat{d}$ deforms continuously with increasing $\vec{j}$ at fixed $\vec{H}$. Not all these configurations can be realized physically, however, and Sec. III investigates the linearized stability of these textures with respect to small variations in the order parameter. For increasing $\vec{j}$ at a given small tipping angle χ, the instability appears at a critical current $j_{0c}(H,\chi)$ that turns out to decrease from the value of $j_{0c}(H,\chi=0)$ approximately like $\chi^{2/3}$. Furthermore, the instability appears at *nonzero* wave vector $\vec{k}_c$ lying in the plane of $\vec{H}$ and $\vec{j}$ (and hence $\hat{l}$ and $\hat{d}$), and with $|k_c| \propto \chi^{2/3}$. Numerical studies for general χ confirm these analytic expressions. Beyond the threshold for the instability, the nonlinear terms in the dynamical equations determine the evolution of the unstable mode. Section IV introduces a general formalism to analyze this behavior, deriving a renormalized Landau-type free energy[7] for the unstable amplitude, with coefficients that depend on the other (still stable) modes. Although the quartic terms in the effective free energy can, in principle, be either positive or negative, an analytic expansion for small χ shows that the resulting instability is catastrophic (an inverted bifurcation).

II. GENERAL FORMALISM

In the hydrodynamic model of the orbital dynamics,[8] the order parameter of ^{3}He-A may be expressed as

$$A_{\mu i}=\Delta d_\mu(\hat{\Delta}_1+i\hat{\Delta}_2)_i \ , \tag{1}$$

where Δ is the maximum magnitude of the energy gap, $\hat{d}$ characterizes the spin of the Cooper pairs, and $\hat{\Delta}_1$ and $\hat{\Delta}_2$ are orthogonal unit vectors with $\hat{l}\equiv\hat{\Delta}_1\times\hat{\Delta}_2$ lying along the orbital angular momentum vector of the Cooper pairs. For the present purpose, it is more convenient to introduce five angles[2] that will serve as the independent dynamical variables: the Euler angles (α,β,γ) of the rigid orthonormal triad $\hat{\Delta}_1,\hat{\Delta}_2,\hat{l}$, and the spherical polar and azimuthal angles (θ,ϕ) of the unit spin vector $\hat{d}$. Given the free-energy density f in the laboratory frame, expressed in terms of these five variables, the dynamical equations take the

form

$$\sin^2\beta\left(\frac{\partial\alpha}{\partial t}+\vec{v}_n\cdot\vec{\nabla}\alpha\right)=-\frac{\delta f}{\delta\alpha}\ , \tag{2}$$

$$\frac{\partial\beta}{\partial t}+\vec{v}_n\cdot\vec{\nabla}\beta=-\frac{\delta f}{\delta\beta}\ , \tag{3}$$

$$\frac{\delta f}{\delta\gamma}=\frac{\delta f}{\delta\theta}=\frac{\delta f}{\delta\phi}=0\ , \tag{4}$$

where $\vec{v}_n$ is the normal fluid velocity. Here, the orbital viscosity has been absorbed into the units of time, and the variational derivatives

$$-\frac{\delta f}{\delta\alpha}\equiv\vec{\nabla}\cdot\frac{\partial f}{\partial\vec{\nabla}\alpha}-\frac{\partial f}{\partial\alpha} \tag{5}$$

are taken holding fixed the other independent variables and their gradients. In the present case, the appropriate free-energy density has $\vec{v}_s$ and $\vec{v}_n$ as its natural variables,[2] with the explicit form[9,10]

$$f=\tfrac{1}{2}\vec{v}_{sn}\vec{\rho}_s\vec{v}_{sn}+\vec{v}_{sn}\vec{C}\,\mathrm{curl}\hat{l}+f_{\mathrm{el}}$$
$$-\tfrac{1}{2}(\hat{l}\cdot\hat{d})^2+\tfrac{1}{2}(\hat{d}\cdot\vec{H})^2-\tfrac{1}{2}\rho v_n^2\ . \tag{6}$$

The tensors $\vec{\rho}_s$ and $\vec{C}$ have uniaxial symmetry along $\hat{l}$, and f_{el} is the elastic energy associated with the deformations of $\hat{l}$ and $\hat{d}$. Furthermore, the Euler angles completely specify the superfluid velocity so that the relative superfluid velocity becomes

$$\vec{v}_{sn}\equiv\vec{v}_s-\vec{v}_n=-\vec{\nabla}\gamma-\cos\beta\vec{\nabla}\alpha-\vec{v}_n\ , \tag{7}$$

with $\vec{v}_n$ taken to be uniform and along $\hat{z}$.

The unit vectors $\hat{l}$ and $\hat{d}$ have the specific form

$$\hat{l}=\sin\beta(\hat{x}\cos\alpha+\hat{y}\sin\alpha)+\hat{z}\cos\beta\ , \tag{8}$$

$$\hat{d}=\sin\theta(\hat{x}\cos\phi+\hat{y}\sin\phi)+\hat{z}\cos\theta\ , \tag{9}$$

and the remaining unit vectors $\hat{\Delta}_1$ and $\hat{\Delta}_2$ may be expressed as

$$\hat{\Delta}_1+i\hat{\Delta}_2=e^{-i\gamma}(\hat{m}+i\hat{n})\ , \tag{10}$$

where

$$\hat{m}=\cos\beta(\hat{x}\cos\alpha+\hat{y}\sin\alpha)-\hat{z}\sin\beta=\frac{\partial\hat{l}}{\partial\beta}\ , \tag{11}$$

$$\hat{n}=-\hat{x}\sin\alpha+\hat{y}\cos\alpha=(\sin\beta)^{-1}\frac{\partial\hat{l}}{\partial\alpha}\ ; \tag{12}$$

they form an orthonormal triad with $\hat{l}$. These angular variables allow us to rewrite the elastic contribution as

$$f_{\mathrm{el}}=\tfrac{1}{2}K_s(\hat{m}\cdot\vec{\nabla}\beta+\sin\beta\hat{n}\cdot\vec{\nabla}\alpha)^2$$
$$+\tfrac{1}{2}K_t(\sin\beta\hat{m}\cdot\vec{\nabla}\alpha-\hat{n}\cdot\vec{\nabla}\beta)^2$$
$$+\tfrac{1}{2}K_b[\sin^2\beta(\hat{l}\cdot\nabla\alpha)^2+(\hat{l}\cdot\vec{\nabla}\beta)^2]$$
$$+\tfrac{1}{2}K_1[(\hat{l}\cdot\vec{\nabla}\theta)^2+\sin^2\theta(\hat{l}\cdot\vec{\nabla}\phi)^2]$$
$$+\tfrac{1}{2}K_2[(\hat{l}\times\vec{\nabla}\theta)^2+\sin^2\theta(\hat{l}\times\vec{\nabla}\phi)^2]\ . \tag{13}$$

The specific geometry of interest involves a uniform hydrodynamic flow $\vec{j}$ along the $\hat{z}$ axis and an external magnetic field $\vec{H}$ lying in the second quadrant of the xz plane at an angle χ (see Fig. 1). A uniform texture requires that $\hat{l}$ and $\hat{d}$ be spatial constants, with the corresponding angles having constant values $\alpha_0, \beta_0, \theta_0, \phi_0$. In contrast, the remaining Euler angle must increase linearly with position, so that

$$\gamma_0=\vec{v}_{s0}\cdot\vec{r}\ , \tag{14}$$

and the uniform relative superfluid velocity, denoted $\vec{v}_0$, becomes

$$\vec{v}_0\equiv\vec{v}_{s0}-\vec{v}_n\ . \tag{15}$$

As a result, the free-energy density for the uniform state is

$$f^0=\tfrac{1}{2}\rho_s v_0^2-\tfrac{1}{2}\rho_0(\hat{l}\cdot\vec{v}_0)^2-\tfrac{1}{2}(\hat{l}\cdot\hat{d})^2$$
$$+\tfrac{1}{2}(\vec{H}\cdot\hat{d})^2-\tfrac{1}{2}\rho v_n^2\ , \tag{16}$$

and the directions of $\hat{l}$ and $\hat{d}$ are determined by minimizing f^0 with respect to the four angles $\alpha_0, \beta_0, \theta_0, \phi_0$. It is easily seen that $\alpha_0=\phi_0=0$, and the remaining equations are[11]

$$H^2\sin(2\theta_0+2\chi)=\sin(2\theta_0-2\beta_0)\ , \tag{17}$$

$$-2\rho_0(\vec{v}_0\cdot\hat{l})(\vec{v}_0\cdot\hat{m})=\sin(2\theta_0-2\beta_0)\ . \tag{18}$$

To interpret this last equation, consider the uniform current (in the frame with $\vec{v}_n=0$)

$$\vec{j}_0=\rho_s\vec{v}_0-\rho_0\hat{l}(\hat{l}\cdot\vec{v}_0) \tag{19}$$

associated with the uniform relative superflow $\vec{v}_0$. In general, $\vec{v}_0$ and $\vec{j}_0$ are not parallel, so that both cannot lie along the z axis. To provide a specific physical picture, imagine flow in a long channel with $\vec{v}_n=v_n\hat{z}$, and transverse bounding walls. Since the physical

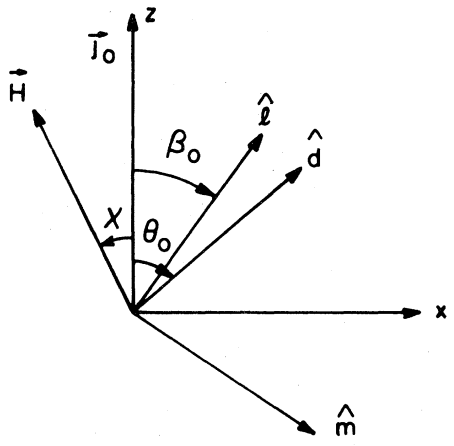

FIG. 1. Orientation of the order parameter for $\vec{H}$ tipped with respect to $\vec{j}_0$. The vector $\hat{n}$ points into the page.

boundary conditions involve the normal component of the current at the boundary, it is natural to insist that $\vec{j}_0$ lie along the flow axis, with

$$\vec{j}_0 = j_0 \hat{z} \ . \tag{20}$$

As a result, $\vec{v}_0$ will have components along both $\hat{z}$ and $\hat{x}$, and straightforward algebra gives the desired scalar products

$$\vec{v}_0 \cdot \hat{l} = \rho_{\parallel}^{-1} \vec{j}_0 \cdot \hat{l} = j_0 \cos\beta_0 / \rho_{\parallel} \ , \tag{21}$$

$$\vec{v}_0 \cdot \hat{m} = \rho_s^{-1} \vec{j}_0 \cdot \hat{m} = -j_0 \sin\beta_0 / \rho_s \ . \tag{22}$$

Explicit elimination of θ_0 then yields

$$\frac{j_0^2 \rho_0}{\rho_s \rho_{\parallel}} \sin 2\beta_0 = \frac{H^2 \sin(2\beta_0 + 2\chi)}{[H^4 - 2H^2 \cos(2\beta_0 + 2\chi) + 1]^{1/2}} \ . \tag{23}$$

If the field is parallel to the flow ($\chi = 0$), Eq. (23) always has the trivial solution $\sin 2\beta_0 = 0$, and the value $\beta_0 = \frac{1}{2}\pi$ is a local minimum of the free energy f^0 for small flow. If j_0 exceeds the value[12]

$$j_* = \left(\frac{\rho_s \rho_{\parallel}}{\rho_0} \right)^{1/2} \frac{H}{(1 + H^2)^{1/2}} \ , \tag{24}$$

the local minimum of f^0 at $\beta_0 = \frac{1}{2}\pi$ changes to a local maximum. Thus the texture tilts uniformly with $\cos\beta_0 \neq 0$. Note that j_* is small for small H and approaches a constant value as $H \to \infty$. Furthermore, the overall coefficient ρ_s/ρ_0 is temperature dependent,[13] decreasing from 2 at $T = T_c$ to ≈ 1.7 at $T = 0.5 T_c$ and then increasing again for lower T because the anisotropy parameter ρ_0 becomes small as $T \to 0$. Although the present analysis provides no information on the stability of the tilted texture with $\beta_0 \neq \frac{1}{2}\pi$, Sec. III will demonstrate that j_* also represents the actual critical current for a dynamical instability when $\chi = 0$. Thus $j_{0c}(\chi = 0)$ should display the characteristic field dependence seen in Eq. (24), and an experimental search for this behavior would be desirable.[14]

Equation (23) has quite different solutions for $\chi \neq 0$. If j_0 vanishes, the stable equilibrium is characterized by the condition $\hat{l} \parallel \hat{d} \perp \vec{H}$, with $\beta_0 = \theta_0 = \frac{1}{2}\pi - \chi$ (see Fig. 1). As j_0 increases from zero at fixed H, both β_0 and θ_0 decrease steadily from $\frac{1}{2}\pi - \chi$, with β_0 ultimately approaching 0 and θ_0 approaching a field-dependent value (≈ 0 if $H \ll 1$ and $\frac{1}{2}\pi - \chi$ if $H \gg 1$). It is not difficult to solve these relations numerically. Figure 2 illustrates a typical case ($\chi = 15°$), showing several lines of constant β_0 in the Hj_0 plane, with the horizontal axis ($j_0 = 0$) denoting the value $\beta_0 = 75°$. The most striking aspect is continuous variation of the orientation angles β_0 and θ_0, in contrast to the finite regions[10] with $\beta_0 = \theta_0 = \frac{1}{2}\pi$ (or 0) that occur for the special value

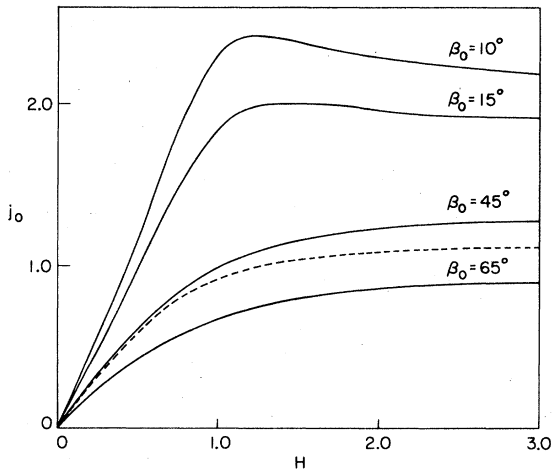

FIG. 2. Phase diagram of the uniform texture for given $\vec{H}$ and $\vec{j}_0$. Here, the tipping angle χ is 15°, and the solid lines denote constant values of β_0. The dashed line is the critical current found numerically in Sec. III.

$\chi = 0$. In general, this paper considers the situation for nonzero χ; that for $\chi = 0$ merely follows as a (not necessarily typical) limit.

It will be important to know the explicit texture for small χ. The previous discussion suggests that the polar angles β_0 and θ_0 should be close to $\frac{1}{2}\pi$ if $j_0 < j_*$, and we therefore assume

$$\theta_0 = \tfrac{1}{2}\pi + \delta\theta, \quad \beta_0 = \tfrac{1}{2}\pi + \delta\beta \quad \text{for } |\chi| \ll 1 \ , \tag{25}$$

with $|\delta\theta|$ and $|\delta\beta| \ll 1$. An expansion of the equilibrium conditions shows that

$$\delta\theta \approx (\delta\beta - H^2\chi)(1 + H^2)^{-1} \ , \tag{26}$$

and

$$\delta\beta \approx -j_*^2 \chi (j_*^2 - j_0^2)^{-1} \ . \tag{27}$$

This last result implies that $\delta\beta$ diverges as $j_0 \to j_*$ from below; as will be seen in Sec. III, however, a dynamical instability renders such singular behavior inaccessible, although it does significantly modify the χ dependence from the linear form shown here.

III. LINEARIZED INSTABILITY OF UNIFORM TEXTURES

The preceding section has determined the uniform (but tilted) equilibrium texture in the presence of a current $\vec{j}_0 = j_0 \hat{z}$ and a magnetic field $\vec{H}$ tipped relative to $\hat{z}$ (see Fig. 1). The next step is to consider the stability of this texture with respect to arbitrary small perturbations (denoted by bars) of the five in-

dependent variables about their equilibrium values [see Eq. (14)]

$$\alpha=\bar{\alpha},\quad \beta=\beta_0+\bar{\beta},\quad \gamma=\gamma_0+\bar{\gamma}\ ,$$
$$\theta=\theta_0+\bar{\theta},\quad \phi=\bar{\phi}\ . \tag{28}$$

Since the resulting linearized dynamical equations will have constant coefficients, the small perturbations $\bar{\alpha},\bar{\beta},\ldots$ can all be taken as plane waves proportional to $e^{i\vec{k}\cdot\vec{r}}$, with $\vec{k}$ an *arbitrary* wave vector. Correspondingly, the analysis will include a complete set of small-amplitude perturbations that fully determine the linearized instability of the uniform texture.

It is important to notice that the dynamical equations form two distinct groups. The variables $\bar{\gamma},\bar{\theta},\bar{\phi}$ obey time-independent equations (4), which, in effect, merely constrain the small-amplitude perturbations. In contrast, Eqs. (2) and (3) involve the time derivatives of $\bar{\alpha}$ and $\bar{\beta}$, in addition to the full set of small amplitudes $\bar{\alpha}$, $\bar{\beta}$, $\bar{\gamma}$, $\bar{\theta}$, and $\bar{\phi}$. As a result, it is convenient to use the linearized equations obtained from Eqs. (4) to eliminate $\bar{\gamma}$, $\bar{\theta}$, and $\bar{\phi}$ explicitly, leading eventually to a set of two coupled equations for $\bar{\alpha}$ and $\bar{\beta}$ that are first order in the time derivatives.

The first step in this procedure is to expand the dynamical equations (4) for θ and ϕ to first order in the small variations. Substitution of the assumed plane-wave form readily yields the results

$$\bar{\phi}=\frac{\cos(\theta_0-\beta_0)\sin\theta_0\sin\beta_0}{\cos(\theta_0-\beta_0)\sin\theta_0\sin\beta_0+H^2\cos(\theta_0+\chi_0)\sin\theta_0\sin\chi+\sin^2\theta_0 K(\vec{k})}\bar{\alpha}\ , \tag{29}$$

$$\bar{\theta}=\frac{\cos(2\theta_0-2\beta_0)}{\cos(2\theta_0-2\beta_0)-H^2\cos(2\theta_0+2\chi)+K(\vec{k})}\bar{\beta}\ , \tag{30}$$

where

$$K(\vec{k})\equiv K_1(\hat{l}\cdot\vec{k})^2+K_2(\hat{l}\times\vec{k})^2\ . \tag{31}$$

As expected from physical considerations, $\bar{\theta}$ invariably vanishes as $H\to\infty$, but $\bar{\phi}$ does so only for $\chi\neq 0$, since otherwise the system is invariant under rotations of $\hat{d}$ about $\hat{z}$.

The corresponding analysis for $\bar{\gamma}$ is more intricate. Inspection of Eq. (6) shows that $\partial f/\partial\gamma=0$, and the dynamical Eq. (4) therefore becomes

$$\vec{\nabla}\cdot\frac{\partial f}{\partial\vec{\nabla}\gamma}=-\vec{\nabla}\cdot\frac{\partial f}{\partial\vec{v}_{sn}}=-\vec{\nabla}\cdot j_0=0\ , \tag{32}$$

where $\vec{j}_0=\partial f/\partial\vec{v}_{sn}$ is again the current in the frame with $\vec{v}_n=0$. To first order in the small quantities, the relative superfluid velocity becomes

$$\vec{v}_{sn}=\vec{v}_0-\vec{\nabla}\bar{\gamma}-\cos\beta_0\vec{\nabla}\bar{\alpha}\ , \tag{33}$$

so that

$$\vec{j}_0\approx\rho_s(\vec{v}_0-\vec{\nabla}\bar{\gamma}-\cos\beta_0\vec{\nabla}\bar{\alpha})-\rho_0\hat{l}[\hat{l}\cdot\vec{v}_0-\hat{l}\cdot(\vec{\nabla}\bar{\gamma}+\cos\beta_0\vec{\nabla}\bar{\alpha})]$$
$$+C(\sin\beta_0\vec{\nabla}\bar{\alpha}\times\hat{n}+\vec{\nabla}\bar{\beta}\times\hat{m})-C_0\hat{l}(\sin\beta_0\hat{m}\cdot\vec{\nabla}\bar{\alpha}-\hat{n}\cdot\vec{\nabla}\bar{\beta})\ . \tag{34}$$

In evaluating Eq. (32), the divergence operator acts not only on the explicit first-order terms, but also on $-\rho_0\hat{l}(\hat{l}\cdot\vec{v}_0)$, which involves $\bar{\alpha}$ and $\bar{\beta}$ through $\hat{l}$ [see Eq. (8)]. The assumed plane-wave dependence allows us to solve the resulting linear equation for $\bar{\gamma}$ explicitly in terms of the variables $\bar{\alpha}$ and $\bar{\beta}$.

The remaining equations (2) and (3) may be expanded in a similar way. Use of Eqs. (29) and (30) and the corresponding one for $\bar{\gamma}$ eventually yields the pair of coupled equations for $\bar{\alpha}$ and $\bar{\beta}$

$$\sin\beta_0\left(\frac{\partial}{\partial t}+i\vec{k}\cdot\vec{v}_n\right)\bar{\alpha}+A(\vec{k})\sin\beta_0\bar{\alpha}+B(\vec{k})\bar{\beta}=0\ , \tag{35}$$

$$\left(\frac{\partial}{\partial t}+i\vec{k}\cdot\vec{v}_n\right)\bar{\beta}+B^*(\vec{k})\sin\beta_0\bar{\alpha}+C(\vec{k})\bar{\beta}=0\ , \tag{36}$$

where

$$A(\vec{k}) = K_s(\hat{n}\cdot\vec{k})^2 + K_t(\hat{m}\cdot\vec{k})^2 + K_b(\hat{l}\cdot\vec{k})^2 + \frac{(\rho_0 j_0\cos\beta_0)^2[(\rho_{\parallel}\rho_s)^{-1}(\hat{l}\cdot\vec{k})^2 + \rho_{\parallel}^{-2}(\hat{m}\cdot\vec{k})^2] - C_0^2(\hat{l}\cdot\vec{k})^2(\hat{m}\cdot\vec{k})^2}{\rho_s k^2 - \rho_0(\hat{l}\cdot\vec{k})^2} + \frac{(\sin\beta_0)^{-1}\cos(\theta_0-\beta_0)\sin\theta_0[H^2\cos(\theta_0+\chi)\sin\theta_0\sin\chi + \sin^2\theta_0 K(\vec{k})]}{\cos(\theta_0-\beta_0)\sin\theta_0\sin\beta_0 + H^2\cos(\theta_0+\chi)\sin\theta_0\sin\chi + \sin^2\theta_0 K(\vec{k})}\ , \tag{37}$$

$$B(\vec{k}) = (K_s-K_t)(\hat{m}\cdot\vec{k})(\hat{n}\cdot\vec{k}) + \frac{C_0^2(\hat{l}\cdot\vec{k})^2(\hat{m}\cdot\vec{k})(\hat{n}\cdot\vec{k}) - \rho_0^2[(\hat{l}\cdot\vec{v}_0)^2(\hat{m}\cdot\vec{k})(\hat{n}\cdot\vec{k}) + (\hat{l}\cdot\vec{v}_0)(\hat{m}\cdot\vec{v}_0)(\hat{l}\cdot\vec{k})(\hat{m}\cdot\vec{k})]}{\rho_s k^2 - \rho_0(\hat{l}\cdot\vec{k})^2} - i\left[\left(2C_0+\rho_{\parallel} - \frac{C_0\rho_{\parallel}(\hat{l}\times\vec{k})^2}{\rho_s k^2-\rho_0(\hat{l}\cdot\vec{k})^2}\right)(\hat{l}\cdot\vec{v}_0)(\hat{l}\cdot\vec{k}) + \rho_s\left(1-\frac{C_0k^2}{\rho_s k^2-\rho_0(\hat{l}\cdot\vec{k})^2}\right)(\hat{m}\cdot\vec{v}_0)(\hat{m}\cdot\vec{k})\right]\ , \tag{38}$$

$$C(k) = K_s(\hat{m}\cdot k)^2 + K_t(\hat{n}\cdot k)^2 + K_b(\hat{l}\cdot k)^2 + \rho_0[(\hat{l}\cdot v_0)^2 - (\hat{m}\cdot v_0)^2] - \frac{C_0^2(\hat{l}\cdot\vec{k})^2(\hat{n}\cdot\vec{k})^2 + \rho_0^2[(\hat{l}\cdot\vec{v}_0)(\hat{m}\cdot\vec{k}) + (\hat{m}\cdot\vec{v}_0)(\hat{l}\cdot\vec{k})]^2}{\rho_s k^2 - \rho_0(\hat{l}\cdot\vec{k})^2} + \frac{\cos(2\theta_0-2\beta_0)[K(\vec{k}) - H^2\cos(2\theta_0+2\chi)]}{\cos(2\theta_0-2\beta_0) + K(\vec{k}) - H^2\cos(2\theta_0+2\chi)} \tag{39}$$

are known functions of the wave vector $\vec{k}$. Here, $\hat{l}$, $\hat{m}$, and $\hat{n}$ have their equilibrium values, and their dot products with $\vec{v}_0$ are given in Eqs. (21) and (22). Since Eq. (34) involves only $\vec{\nabla}\vec{\gamma}$, the case $\vec{k}=0$ requires slightly different treatment, but the resulting values $A(0)$, $C(0)$ are not needed here [$B(0)$ vanishes].

Equations (35) and (36) have simple exponential solutions of the form $e^{\sigma t}$. Direct substitution leads to the eigenvalue condition for $\Omega \equiv \sigma + i\vec{k}\cdot\vec{v}_n$

$$(\Omega + A)(\Omega + C) - |B|^2 = 0 \tag{40}$$

with the real roots

$$\Omega^{(1)} = -\tfrac{1}{2}(A+C) + [\tfrac{1}{4}(A+C)^2 + |B|^2 - AC]^{1/2}\ , \tag{41}$$

$$\Omega^{(2)} = -\tfrac{1}{2}(A+C) - [\tfrac{1}{4}(A+C)^2 + |B|^2 - AC]^{1/2}\ . \tag{42}$$

The real expressions A and C are generally positive, so that $\Omega^{(2)}(\vec{k})$ is always negative and the corresponding normal modes are stable. On the other hand, the root $\Omega^{(1)}(\vec{k})$ has the sign of $|B|^2 - AC$. This quantity turns out to have a maximum value for some *nonzero* $\vec{k}$. If j_0 is small, this maximum will be negative, so that the associated uniform but tilted texture is stable with respect to arbitrary small perturbations. As j_0 increases at fixed H, however, two things happen. First, the vectors $\hat{l}$ and $\hat{d}$ rotate uniformly in the plane of j_0 and H, maintaining the equilibrium configuration derived in Sec. II. Second, the maximum of $|B(\vec{k})|^2 - A(\vec{k})C(\vec{k})$ increases and passes through zero at the critical value j_{0c} of the current; this represents the onset of a dynamical instability with finite wave vector $\vec{k}_c$. For $j_0 \gtrsim j_{0c}$, the normal modes associated with the eigenvalue $\Omega^{(1)}(\vec{k})$ will display exponential growth for wave vectors in some small region around $\vec{k}_c$. This behavior is typical of a bifurcation, familiar in hydrodynamics,[15,16] but nonlinear corrections (Sec. IV) are required to determine the precise character of the instability.

In practice, the expressions in Eqs. (37)–(39) are complicated functions of the wave vector $\vec{k}$ and the current j_0 for a given magnetic field H and tipping angle χ. Thus the maximization of $|B(\vec{k})|^2 - A(\vec{k})C(\vec{k})$ presents a difficult problem that must be treated numerically. If χ is small, however, an analytic expansion becomes feasible. Since the resulting critical current also serves to check the numerical

analysis, the small-χ expansion will be presented in some detail.

One important simplification is possible, for numerical studies indicate that the local maximum of $|B|^2 - AC$ occurs for $\vec{k}$ in the xz plane, so that $\hat{n} \cdot \vec{k}$ vanishes. Furthermore, if $\chi = 0$, the instability can be shown to occur at long wavelengths ($k_c \to 0$), with k essentially along the x axis. Consequently, $|\vec{k}_c|$ for $|\chi| \ll 1$ is expected to be small, and its polar angle ψ relative to $\hat{z}$ should be near $\frac{1}{2}\pi$. If this angle is written as $\psi = \frac{1}{2}\pi + \delta\psi$ with $\delta\psi$ small, the quantity $A(\vec{k})$ has the approximate form

$$A(\vec{k}) \approx (K_b + K_1)k^2 + \frac{j_0^2 \rho_0}{\rho_s \rho_{\parallel}} \frac{j_*^2}{j_*^2 - j_0^2} \times \left(1 + \frac{\rho_0}{\rho_{\parallel}} \frac{j_*^2}{j_*^2 - j_0^2}\right)\chi^2 \ , \tag{43}$$

where j_* is the critical current for $\chi = 0$ [see Eq. (24)]. Since the critical current j_{0c} for small χ should differ only slightly, it is natural to write

$$j_0^2 = j_*^2(1-\delta) = \frac{\rho_s \rho_{\parallel}}{\rho_0} \frac{H^2}{1+H^2}(1-\delta) \ , \tag{44}$$

where $\delta \ll 1$. As a result, Eq. (43) reduces to

$$A(\vec{k}) \approx (K_b + K_1)k^2 + \frac{H^2}{1+H^2} \frac{\rho_0}{\rho_{\parallel}} \frac{\chi^2}{\delta^2} \ , \tag{45}$$

apart from corrections of relative order δ. Similarly, $B(\vec{k})$ and $C(\vec{k})$ have the approximate forms

$$B(\vec{k}) \approx \frac{ikj_0}{\rho_{\parallel}} [3C_0 \delta\beta + (\rho_{\parallel} - C_0)\delta\psi] \ , \tag{46}$$

$$C(\vec{k}) \approx \left(K_b + \frac{K_1}{(1+H^2)^2}\right)k^2 + \frac{H^2}{1+H^2}\left(\delta + \frac{\rho_0}{\rho_{\parallel}}(2\delta\beta - \delta\psi)^2\right) + \frac{6H^4}{(1+H^2)^3}(\delta\beta)^2 \ . \tag{47}$$

Near T_c, the hydrodynamic parameters satisfy the relation $C_0 = \rho_{\parallel}$, in which case $\delta\psi$ appears only in $C(\vec{k})$. The corresponding maximum of $|B|^2 - AC$ with respect to variations in $\delta\psi$ then occurs for $\delta\psi = 2\delta\beta$; hence the direction of the critical wave vector $\vec{k}_c$ near T_c differs from that of $\hat{l}$, for $\vec{k}_c$ is obtained by rotating precisely twice as far from the x axis [see Fig. 3(a)]. More generally, it is convenient to approximate $C_0 - \rho_{\parallel} \approx 0$ and $\delta\psi \approx 2\delta\beta$ for small χ throughout the A phase, because the quantity $C_0 - \rho_{\parallel}$ is always small.

The remaining problem is to determine the magnitude of k that maximizes $|B|^2 - AC$. A combination

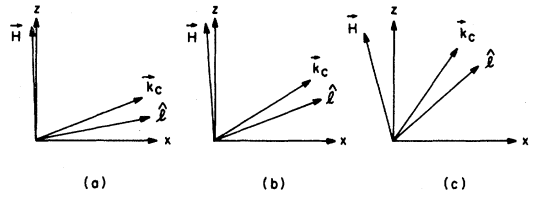

FIG. 3. Relative orientation of order parameter and critical wave vector for small H with $\chi =$ (a) 1°, (b) 5°, and (c) 15°.

of Eqs. (27) and (44) shows that

$$\delta\beta = -\chi/\delta \ , \tag{48}$$

and the assumption that $\delta\beta \ll 1$ requires the additional condition $\chi \ll \delta \ll 1$. Use of Eq. (48) and setting $\delta\psi = 2\delta\beta$ leads to the following quadratic expression for k^2

$$|B(\vec{k})|^2 - A(\vec{k})C(\vec{k}) = -Xk^4 + Yk^2 \frac{H^2}{1+H^2} - Z\frac{H^4}{(1+H^2)^2} \ , \tag{49}$$

where

$$X = (K_b + K_1)[K_b + K_1(1+H^2)^{-2}] \ , \tag{50}$$

$$Y = \frac{9\rho_s \rho_{\parallel}}{\rho_0}\frac{\chi^2}{\delta^2} - (K_b + K_1)\left(\delta + \frac{6H^2}{(1+H^2)^2}\frac{\chi^2}{\delta^2}\right) - \frac{\rho_0}{\rho_{\parallel}}\frac{\chi^2}{\delta^2}\left(K_b + \frac{K_1}{(1+H^2)^2}\right) \ , \tag{51}$$

$$Z = \frac{\rho_0}{\rho_{\parallel}}\frac{\chi^2}{\delta^2}\left(\delta + \frac{6H^2}{(1+H^2)^2}\frac{\chi^2}{\delta^2}\right) \ . \tag{52}$$

Since X and Z are positive, the maximum occurs at the nonzero wave number

$$k_c^2 = \frac{Y}{2X}\frac{H^2}{1+H^2} \tag{53}$$

if $Y > 0$, and the corresponding maximum value is

$$(|B|^2 - AC)_{\max} = \frac{1}{4X}\frac{H^4}{(1+H^2)^2}(Y^2 - 4XZ) \ . \tag{54}$$

For negative $Y^2 - 4XZ$, all normal modes are stable, so that the onset of instability is determined by the condition

$$Y^2 - 4XZ = 0 \ , \tag{55}$$

which is a quadratic form in the variables δ and $(\chi/\delta)^2$. Hence it is natural to assume that δ_c at the onset of instability has the form

$$\delta_c = \lambda\chi^{2/3} \ . \tag{56}$$

Equation (55) then becomes

$$\chi^{2/3}(\hat{Y}^2 - 4\hat{X}\hat{Z}) = 0 \ , \tag{57}$$

where quantities with a circumflex are obtained from Eqs. (50)–(52) with the substitutions $\delta \to \lambda$ and $(\chi/\delta)^2 \to \lambda^{-2}$. For given values of the hydrodynamic parameters, Eq. (57) determines the constant λ as a function of the applied field H. In particular, the weak-coupling values

$$\rho_{\parallel} = \rho_0 = \tfrac{1}{2}\rho_s = K_1 = \tfrac{2}{3}K_b = 1$$

yield the behavior shown in Fig. 4; it is evident that λ is nearly independent of H and of order 1.

It is now possible to determine the physical quantities that characterize the onset of instability of the uniform texture for small χ. First, Eqs. (44) and (56) give the critical current

$$j_{0c}^2 = \frac{\rho_s \rho_{\parallel}}{\rho_0}\frac{H^2}{1+H^2}(1-\lambda\chi^{2/3}) \ , \tag{58}$$

which is reduced from that for $\chi = 0$ by a nonanalytic correction of order $\chi^{2/3}$. Second, the vectors $\hat{d}$ and $\hat{l}$ are rotated from the x axis by the small angles [see Eqs. (26) and (48)]

$$\delta\theta_c \approx \delta\beta_c(1+H^2)^{-1} \approx -\chi^{1/3}\lambda^{-1}(1+H^2)^{-1} \ , \tag{59a}$$

$$\delta\beta_c \approx -\chi^{1/3}\lambda^{-1} \ , \tag{59b}$$

respectively (the minus sign means a rotation toward the z axis). Third, the instability occurs for a small-amplitude plane-wave perturbation $\propto e^{i\vec{k}_c\cdot\vec{r}}$, with a wave vector $\vec{k}_c$ lying in the xz plane at an angle $\approx 2\delta\beta$ relative to the x axis [see Fig. 3(a)] and a *nonzero* magnitude given by

$$k_c^2 \approx \frac{\hat{Y}}{2\hat{X}}\frac{H^2\chi^{2/3}}{1+H^2}, \quad \chi \ll 1 \ . \tag{60}$$

Here, the coefficient $\hat{Y}/\hat{X}$ varies slowly with H and is of order 1. Finally, the quantities $A(\vec{k}_c)$, $|B(\vec{k}_c)|$, and $C(\vec{k}_c)$ are all of order $H^2\chi^{2/3}(1+H^2)^{-1}$. Therefore, the normalized eigenvector

$$u^{(1)}(\vec{k}_c) \equiv \begin{pmatrix} \sin\beta_0\bar{\alpha}^{(1)} \\ \bar{\beta}^{(1)} \end{pmatrix} = (C^2+|B|^2)^{-1/2}\begin{pmatrix} C(\vec{k}_c) \\ -B^*(\vec{k}_c) \end{pmatrix} \tag{61}$$

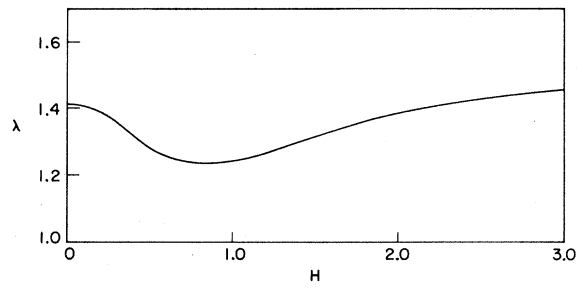

FIG. 4. Dependence of the parameter λ [see Eq. (56)] on the applied magnetic field.

associated with the normal-mode eigenvalue $\Omega^{(1)}(\vec{k}_c) \approx 0$ has both components of order unity. The unstable mode introduces the perturbation

$$\delta\hat{l}(t) \propto \mathrm{Re}\{[C(\vec{k}_c)\hat{n} - B^*(\vec{k}_c)\hat{m}]\exp(i\vec{k}_c\cdot\vec{r})\} \times \exp[\Omega^{(1)}(\vec{k}_c)t] \tag{62}$$

lying in the plane perpendicular to $\hat{l}$. Since $B(\vec{k}_c)$ is pure imaginary but $|B(\vec{k}_c)| \neq C(\vec{k}_c)$, the tip of the vector $\delta\hat{l}$ traces out a slightly deformed spiral with its axis oriented along the direction $\hat{k}_c$. It is notable that $\hat{k}_c$ can differ considerably from $\hat{l}$, which confirms the importance of including full three-dimensional perturbations with general $\vec{k}$, as opposed to a restricted set, such as longitudinal or transverse with respect to a particular direction.[1–3]

The preceding analysis shows that the case $\chi = 0$ ($\vec{H}$ parallel to $j\hat{z}$) is special, for the instability then occurs at $\vec{k}_c = 0$. To study this situation in detail, it is necessary to impose a large but finite quantization length L on the allowed wave numbers $\vec{k} = 2\pi L^{-1}(n_1, n_2, n_3)$, with $L \gg 1$ (measured in units of L^*, see Ref. 9). For given H, the texture remains uniform with $\beta_0 = \theta_0 = 90°$ for all $j_0 < j_*$ [see Eq. (24)]. Precisely at j_*, the vectors $\hat{l}$ and $\hat{d}$ start to rotate away from the x axis, remaining uniform and in the xz plane. This deformation does not proceed very far, however, for when $\cos^2\beta_0 \approx (\delta\beta)^2$ is of order L^{-2} [see Eq. (25)], the uniform texture becomes dynamically unstable with respect to a plane-wave deformation with $\vec{k}_c \approx 2\pi L^{-1}(\hat{x} + 2\delta\beta\hat{z})$. Since $L \gg 1$, these two closely spaced transitions will typically remain unresolved in most experiments, and the uniform texture with $\chi = 0$ and $\hat{l} = \hat{d} = \hat{x}$ will appear to become dynamically unstable at $j_0 \approx j_*$.

Numerical studies for several nonzero values of χ confirmed these analytic expansions. In particular, the instability invariably occurs at a finite wave vector $\vec{k}_c$ that differs in direction from $\hat{l}$ (see Fig. 3). When χ is small, the directions of $\vec{k}_c$ and $\hat{l}$ at the onset of instability are essentially independent of H, in agreement with Eq. (59) and the discussion below Eq. (47). For larger χ (15°, for example), β_0 at $\vec{k}_c$ increases appreciably with increasing H. The dashed line (the critical current) in Fig. 2 illustrates this behavior; it is clear that this curve crosses lines of constant β_0, but the net change is small in going from $H = 0$ (where $\beta_0 \approx 48°$) to $H = 3$ (where $\beta_0 \approx 55°$). In addition, $|\vec{k}_c|$ increases with increasing H at a given χ and also with increasing χ, although the dependence for large χ is more complicated than in Eq. (60). Most interesting is the critical current $j_{0c}(H)$, which is shown in Fig. 5 for several values of χ. As anticipated from Eq. (58), j_{0c} at fixed H initially decreases with increasing χ, but the behavior for larger χ is more complicated (for example, the curves for $\chi = 5$ and 15° cross near $H = 1$). The conclusion both of the expansions and of the numerical

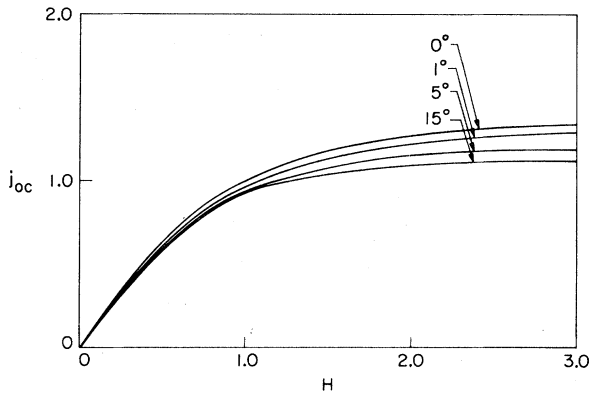

FIG. 5. Dependence of the critical current on magnetic field for several values of the tipping angle χ.

studies is that the uniform texture in a magnetic field undergoes a dynamical plane-wave instability with a finite wave number. The present linearized theory cannot predict the long-time fate of the unstable normal mode, which instead requires a detailed nonlinear analysis.

IV. NONLINEAR DYNAMICS NEAR THE INSTABILITY

To study the nonlinear dynamics of the texture, it is convenient to rewrite Eqs. (2)–(4) in a more compact form by introducing two separate column vectors

$$u=\begin{pmatrix}\sin\beta_0\bar{\alpha}\\ \bar{\beta}\end{pmatrix},\quad v=\begin{pmatrix}\bar{\gamma}\\ \bar{\theta}\\ \bar{\phi}\end{pmatrix}, \tag{63}$$

with components labeled by the index $i,j,\ldots,$ and $a,b,\ldots,$ respectively. They include only the *deviations* from the uniform equilibrium values, as given in Eq. (28). To simplify the resulting expressions, spatial gradients of u and v will be denoted by Greek indices, for example $u_{i\lambda}=\partial u_i/\partial x_\lambda$. In addition, it is natural to introduce plane-wave expansions of the form

$$u_i(\vec{r},t)=V^{-1/2}\sum_{\vec{p}} e^{i\vec{p}\cdot\vec{r}}u_i(\vec{p},t)\ , \tag{64}$$

with $u_i(-\vec{p})=u_i(\vec{p})^*$. Finally, the total free energy $F=\int d^3r\, f$ may be expanded in powers of u and v about the uniform equilibrium texture

$$F=F^{(0)}+F^{(1)}+F^{(2)}+\cdots\ , \tag{65}$$

where [see Eq. (16)]

$$F^{(0)}=Vf^0\ , \tag{66a}$$

$$F^{(1)}=V^{1/2}[f_iu_i(\vec{p}=0)+f_av_a(\vec{p}=0)]\ , \tag{66b}$$

$$F^{(2)}=\tfrac{1}{2}\sum_{\vec{p}_1,\vec{p}_2}\delta_{\vec{p}_1,-\vec{p}_2}[P_{jk}(\vec{p}_1,\vec{p}_2)u_j(\vec{p}_1)u_k(\vec{p}_2)+2P_{ja}(\vec{p}_1,\vec{p}_2)u_j(\vec{p}_1)v_a(\vec{p}_2)+P_{ab}(\vec{p}_1,\vec{p}_2)v_a(\vec{p}_1)v_b(\vec{p}_2)]\ , \tag{66c}$$

with summations over repeated indices. Here, the coefficients in the first-order terms are the first derivatives of the free-energy density [Eq. (6)] evaluated at equilibrium

$$f_i=\left(\frac{\partial f}{\partial u_i}\right)_0,\quad f_a=\left(\frac{\partial f}{\partial v_a}\right)_0\ . \tag{67}$$

The quantities $P_{ij}(\vec{p}_1,\vec{p}_2)$ appearing in $F^{(2)}$ are given by

$$P_{jk}(\vec{p}_1,\vec{p}_2)=f_{j,k}+ip_{2\lambda}f_{j,k\lambda}+ip_{1\lambda}f_{j\lambda,k}-p_{1\lambda}p_{2\mu}f_{j\lambda,k\mu}\ , \tag{68}$$

where the Greek indices again represent spatial components, and the coefficients are second derivatives of f, evaluated at equilibrium

$$f_{j,k}=\left(\frac{\partial^2 f}{\partial u_j\partial u_k}\right)_0,\quad f_{j,k\lambda}=f_{k\lambda,j}=\left(\frac{\partial^2 f}{\partial u_j\partial u_{k\lambda}}\right)_0,\quad f_{j\lambda,k\mu}=\left(\frac{\partial^2 f}{\partial u_{j\lambda}\partial u_{k\mu}}\right)_0\ , \tag{69}$$

and similarly with $u_j\cdots$ replaced by $v_a\cdots$.

The exact dynamical equations follow from Eqs. (2)–(4). It is useful to introduce a diagonal matrix

$$M=(\sin^2\beta_0)^{-1}\begin{pmatrix}\sin^2\beta & 0\\ 0 & \sin^2\beta_0\end{pmatrix} \tag{70}$$

and then to expand it in powers of u

$$M_{ij}=\delta_{ij}+M^{(1)}_{ijk}u_k+\tfrac{1}{2}M^{(2)}_{ijkl}u_ku_l+\cdots\ . \tag{71}$$

The Fourier components of u and v obey the equations of motion

$$0=-\frac{\partial F}{\partial v_a(-\vec{k})}\ , \tag{72}$$

$$\left(\frac{\partial}{\partial t}+iv_{n\lambda}k_\lambda\right)u_i(\vec{k})+V^{-1/2}\sum_{\vec{p}}M^{(1)}_{ijk}\left[\left(\frac{\partial}{\partial t}+iv_{n\lambda}p_\lambda\right)u_j(\vec{p})\right]u_k(\vec{k}-\vec{p})+\tfrac{1}{2}V^{-1}\sum_{\vec{p},\vec{q}}M^{(2)}_{ijkl}\left[\left(\frac{\partial}{\partial t}+iv_{n\lambda}p_\lambda\right)u_j(\vec{p})\right]u_k(\vec{q})u_l(\vec{k}-\vec{p}-\vec{q})+\cdots=-\frac{\partial F}{\partial u_i(-\vec{k})}\ , \tag{73}$$

which explicitly recognize the different roles of u and v. The zero-order contributions require that the quantities in Eq. (67) vanish, which are just the equilibrium conditions (17) and (18). To treat the first- and higher-order contributions, however, it is simplest to solve Eq. (72) directly for $v_a(\vec{k})$ as a power series in u_i. Since F is stationary with respect to v, this solution may be substituted back into Eq. (65) to yield an effective free energy that depends only on the dynamical variables u_i. A detailed calculation leads to the expansion

$$F = VF^{(0)} + \frac{1}{2}\sum_{\vec{p}_1,\vec{p}_2}\delta_{\vec{p}_1+\vec{p}_2,0}N_{ij}(\vec{p}_1,\vec{p}_2)u_i(\vec{p}_1)u_j(\vec{p}_2)$$
$$+\frac{1}{6}V^{-1/2}\sum_{\vec{p}_1,\vec{p}_2,\vec{p}_3}\delta_{\vec{p}_1+\vec{p}_2+\vec{p}_3,0}N_{ijk}(\vec{p}_1,\vec{p}_2,\vec{p}_3)u_i(\vec{p}_1)u_j(\vec{p}_2)u_k(\vec{p}_3)$$
$$+\frac{1}{24}V^{-1}\sum_{\vec{p}_1,\vec{p}_2,\vec{p}_3,\vec{p}_4}\delta_{\vec{p}_1+\vec{p}_2+\vec{p}_3+\vec{p}_4,0}N_{ijkl}(\vec{p}_1,\vec{p}_2,\vec{p}_3,\vec{p}_4)u_i(\vec{p}_1)u_j(\vec{p}_2)u_k(\vec{p}_3)u_l(\vec{p}_4)+\cdots , \quad (74)$$

where the coefficients are totally symmetric under the interchange of any pair of indices

$$N_{ijk}\cdots(\vec{p}_1,\vec{p}_2,\vec{p}_3,\ldots) = N_{jik}\cdots(\vec{p}_2,\vec{p}_1,\vec{p}_3,\ldots) \quad (75)$$

and satisfy the complex-conjugation relations

$$N_{ij}\ldots(\vec{p}_1,\vec{p}_2,\ldots)^* = N_{ij}\ldots(-\vec{p}_1,-\vec{p}_2,\ldots) . \quad (76)$$

Their detailed form is quite complicated, and only the leading one is needed

$$N_{ij}(-\vec{p},\vec{p}) = P_{ij}(-\vec{p},\vec{p}) - P_{ia}(-\vec{p},\vec{p}) \times [P(-\vec{p},\vec{p})^{-1}]_{ab}P_{bj}(-\vec{p},\vec{p}) . \quad (77)$$

Here the matrix indices a and b run over the values 1,2,3 if $\vec{p}\neq 0$, but only over 2 and 3 if $\vec{p}=0$ [compare the discussion below Eq. (39)]. The resulting dynamical equations for u can be simplified with the substitution

$$u_j(\vec{p},t) = \exp(-iv_{n\lambda}p_\lambda t)\bar{u}_j(\vec{p},t) \quad (78)$$

but the overbar will be omitted. In this way, the modified two-component column vector obeys the same dynamical equation (73) with $v_n=0$ and with the right-hand side evaluated for the effective free energy in Eq. (74).

To first order in u, these equations become

$$\frac{\partial u_i(\vec{k},t)}{\partial t} + N_{ij}(-\vec{k},\vec{k})u_j(\vec{k},t) = 0 , \quad (79)$$

which merely restates the linear Eqs. (35) and (36) found previously, since it is easy to show that

$$N_{11}(-\vec{k},\vec{k}) = A(\vec{k}),\quad N_{12}(-\vec{k},\vec{k}) = B(\vec{k}) ,$$
$$N_{22}(-\vec{k},\vec{k}) = C(\vec{k}) .$$

The introduction of normal coordinates $\zeta_i(\vec{k},t)$ can simplify the subsequent analysis.[17] Construct the (time-independent) modal matrix $\mathfrak{A}(\vec{k})$ from the two eigenvectors of $N(-\vec{k},\vec{k})$ and then write

$$u_i(\vec{k},t) = \mathfrak{A}_{ij}(\vec{k})\zeta_j(\vec{k},t) . \quad (80)$$

As is familiar from classical mechanics, the modal matrix here turns out to be unitary and it also diagonalizes the matrix N_{ij} through the relations

$$[\mathfrak{A}^\dagger(\vec{k})\mathfrak{A}(\vec{k})]_{ij} = \delta_{ij} ,$$
$$[\mathfrak{A}^\dagger(\vec{k})N(-\vec{k},\vec{k})\mathfrak{A}(\vec{k})]_{ij} = -\delta_{ij}\Omega^{(i)}(\vec{k}) . \quad (81)$$

Thus Eq. (79) assumes the more transparent form

$$\frac{\partial\zeta_i(\vec{k},t)}{\partial t} = \Omega^{(i)}(\vec{k})\zeta_i(\vec{k},t) . \quad (82)$$

If the current j_0 is near the critical value j_{0c}, then the eigenvalue $\Omega^{(1)}(\vec{k})$ has a local maximum at $\vec{k}_c$ (see Sec. III) that is positive or negative according to the sign of j_0-j_{0c}. Thus $\Omega^{(1)}(\vec{k})$ in the vicinity of $\vec{k}_c$ has the approximate form

$$\Omega^{(1)}(\vec{k}) \approx \Omega^{(1)}(\vec{k}_c) - (k-k_c)_\lambda(k-k_c)_\mu\Omega_{\lambda\mu} + \cdots , \quad (83)$$

where $\Omega_{\lambda\mu}$ is a positive-definite real symmetric matrix. For small positive j_0-j_{0c}, the condition $\Omega^{(1)}(\vec{k})=0$ defines an ellipsoidal region in k space whose typical dimension will be denoted $\epsilon(\ll 1)$. Correspondingly, $\Omega^{(1)}(\vec{k}_c)$ is of order ϵ^2, and the substitution $\vec{k}=\vec{k}_c+\epsilon\vec{w}$ brings Eq. (83) to the form

$$\Omega^{(1)}(\vec{w}) \approx \epsilon^2(s\,\Omega - w_\lambda w_\mu\Omega_{\lambda\mu}) , \quad (84)$$

where $s\equiv\mathrm{sgn}(j_0-j_{0c})$; this expression holds both above and below threshold, assuming only that $|j_0-j_{0c}|\approx O(\epsilon^2 j_{0c})$. In contrast, modes for $i=2$ or with $\vec{k}$ far from $\vec{k}_c$ have $\Omega^{(i)}(\vec{k})$ negative and of order 1.

To clarify the behavior of the unstable modes $\zeta_1(\vec{k},t)$ for $\vec{k}$ near $\vec{k}_c$, it is useful to give them a special symbol

$$\psi(\vec{w}) \equiv \epsilon\zeta_1(\vec{k}_c+\epsilon\vec{w}) , \quad (85)$$

where the explicit factor ϵ reflects the small amplitude beyond a normal bifurcation.[15] Since $\psi(\vec{w})$ is expected to exhibit a slow time dependence, it is also helpful to introduce the scaled time variable[16,18,19]

$$\tilde{t} = \epsilon^2 t . \quad (86)$$

The remaining modes with $i=2$ or with $\vec{k}$ far from $\vec{k}_c$ would decay spontaneously in the linearized approximation. For the nonlinear theory, however, they are driven by the unstable modes $\psi(\vec{w})$ and turn out to be of order ϵ^2. Systematic elimination of these other modes[20,21] leads to the final form

$$\frac{\partial\psi(\vec{w})}{\partial\tilde{t}} = (s\Omega - w_\lambda w_\mu \Omega_{\lambda\mu})\psi(\vec{w}) + \frac{\Gamma}{V}\sum_{\vec{w}',\vec{w}''}\psi(\vec{w}')\psi(\vec{w}'') \times \psi(-\vec{w}+\vec{w}'+\vec{w}'')^* \ , \quad (87)$$

where Γ depends only on $\vec{k}_c$ to lowest order[22] in ϵ

$$2\Gamma \approx -\sum_j \left(\frac{|\bar{N}_{11j}(-\vec{k}_c,-\vec{k}_c,2\vec{k}_c)|^2}{\Omega^{(j)}(2\vec{k}_c)} + 2\frac{|\bar{N}_{11j}(-\vec{k}_c,\vec{k}_c,\vec{0})|^2}{\Omega^{(j)}(\vec{0})} \right) - \bar{N}_{1111}(-\vec{k}_c,\vec{k}_c,\vec{k}_c,-\vec{k}_c) \ , \quad (88)$$

and $\bar{N}_{ijk}\ldots$ denotes the projection of $N_{ijk}\ldots$ onto the appropriate eigenvectors. Note that the first two terms of Γ are positive definite because $\Omega^{(j)}(2\vec{k}_c)$ and $\Omega^{(j)}(0)$ are negative (modes with $\vec{k}$ far from $\vec{k}_c$ are stable). The last term in Eq. (89) can have either sign, however, and Γ can therefore, in principle, be positive or negative.

Suppose that ϵ is so small that only the single mode at $\vec{k}_c$ has become unstable. The sum in Eq. (88) then reduces to a single term with $\vec{w}=\vec{w}'=\vec{w}''=0$, and the resulting equation for $\psi(\vec{0})$ exhibits a normal (inverted) bifurcation if Γ is negative (positive). In the former case, the solution $\psi(\vec{0})=0$ is stable below threshold ($s=-1$), whereas the solution $|\psi|^2 = V\Omega/|\Gamma|$ is stable above ($s=1$). More unusual is the case of positive Γ, when the solution $\psi(\vec{0})=0$ is again stable below threshold, but only for initial conditions $|\psi|^2 < V\Omega/\Gamma$. Above threshold ($s=1$), in contrast, $\psi(\vec{0})$ in this approximation increases without limit for any initial conditions, and the present expansion of the free energy through fourth order in u is incapable of determining the long-time behavior of the unstable normal mode. It is interesting that both of these situations arise in the study of helical textures[1-3] in ^{3}He-A, subject to an increasing H field parallel to the external flow. For small H, the uniform texture is stable. At a critical value H_0, it undergoes a normal bifurcation to a helical deformation with finite wave number. In this case, the first term of Eq. (88) vanishes identically, and the remaining contribution ensures that $\Gamma<0$. The periodic texture then evolves with increasing $H-H_0$ until a second critical field H_1, when the helix itself becomes unstable with respect to long-wavelength perturbations ($k_c \to 0$). In this latter transition, it is not hard to verify that the first term of Eq. (88) predominates, with the remainder being of higher order in the small parameter k_c.

The preceding formalism applies directly to the instability studied in Sec. III. In general, determining the sign and magnitude of Γ requires a lengthy numerical investigation, since it involves the full set of third and fourth derivatives of the original free-energy density, evaluated at the threshold for the instability (with the finite wave vector $\vec{k}_c$). Fortunately, however, the situation becomes much simpler for small tipping angles χ between H and the applied current $j_0\hat{z}$. In this case, it is not difficult to see that $\Omega^{(j)}(\vec{k}\approx 2\vec{k}_c)$ and $\Omega^{(j)}(\vec{k}\approx\vec{0})$ are of order k_c^2 for both values of j. Furthermore the quantities $\bar{N}$ in Eq. (88) approach finite limits as χ (and hence k_c^2) tends toward zero. Consequently, the first two terms in Eq. (88) predominate, and Γ becomes large like $\chi^{-2/3}(1+H^{-2})$; this result immediately implies that *for small tipping angles χ, the instability associated with the critical current j_{0c} in Eq. (58) represents an inverted bifurcation,* with the amplitude of the unstable modes subject to rapid and catastrophic growth beyond threshold. The ultimate behavior depends on higher-order terms in the free energy and may not even be accessible through any finite-order expansion in the (assumed small) displacement u_i.

V. DISCUSSION

The present paper has considered the dynamics of bulk uniform superfluid ^{3}He-A in the presence of a uniform magnetic field $\vec{H}$ and then subjected to an adiabatically increasing hydrodynamic flow $\vec{j}_0$. If $\vec{H}$ is parallel to $\vec{j}_0$, the instability of the uniform configuration ($\hat{l}=\hat{d}=\hat{x}$) occurs for long wavelengths at a critical current

$$j_* = (\lambda_D \rho_s \rho_{\parallel}/\rho_0)^{1/2} H(1+H^2)^{-1/2} \ ,$$

here given in conventional units, with H measured in units of $H^* = (\lambda_D/\lambda_M)^{1/2} \approx 30$ Oe. The corresponding critical velocity is j_*/ρ_s. A very different situation occurs if $\vec{H}$ and $\vec{j}_0$ have a nonzero angle χ between them. Although a uniform texture is again stable up to a critical current j_{0c}, the instability now appears at a wave vector $\vec{k}_c$, with finite magnitude of order $\chi^{1/3}H(1+H^2)^{-1/2}$ for $\chi \ll 1$, and lying in the plane of $\vec{H}$ and $\vec{j}_0$, but not along $\hat{l}$. Furthermore, the critical current for nonzero χ is reduced from that for $\chi=0$, by an amount proportional to $\chi^{2/3}H^2(1+H^2)^{-1}$ for $\chi \ll 1$. Finally, a detailed analysis of the nonlinear dynamics beyond threshold indicates that the instability for $\chi \ll 1$ is an inverted bifurcation, in which the amplitudes of the leading unstable modes grow rapidly with time rather than saturating at some nearby state. The present calcula-

tion cannot decide whether this rapidly changing texture will eventually attain a new static equilibrium or, instead, continue to execute some complicated dynamical trajectory with a corresponding continuous dissipation of energy.

Several experiments have studied the hydrodynamic properties of superfluid ^{3}He-A in an applied magnetic field. Bagley *et al.*[23] used a torsion pendulum with a relatively large flow velocity ($\gtrsim 1$ mm/sec) and an unspecified residual magnetic field following demagnetization. Since these flows probably exceeded the critical velocity, they presumably observed only the dissipative regime beyond threshold. More recently, Dahm *et al.*[24] used a capacitance method to drive the fluid through a superleak with an applied perpendicular magnetic field of ≈ 100 Oe. Unfortunately, the predicted evolution of the texture in such a configuration ($\vec{H} \perp \vec{v}_s$) is quite different[1] from that considered here, so that these experimental data cannot be compared with our calculations. The most pertinent experiments are those by Paalanen and Osheroff,[5] who used large H parallel to the superflow ($\chi = 0$). They indeed observed a critical velocity v_c in superfluid ^{3}He-A, but the magnitude is only about 0.6 of the value $(\lambda_D \rho_{\parallel}/\rho_s \rho_0)^{1/2}$ found here in the limit $H \gg 1$. Above v_c, a pressure head appeared, indicating the presence of dissipation. It is natural to ask whether these observed phenomena have any relation to those predicted by the present theory. In this context, several remarks are relevant.

(1) The observed v_c depended on magnetic field, decreasing for $H \lesssim 40$ Oe, but more detailed studies would be needed to check the predicted $H(1+H^2)^{-1/2}$ dependence.

(2) The critical current at small tipping angle χ could provide a decisive test, for it is predicted to display a characteristic dependence on χ and H. (The velocity is less simple, because the anisotropy of $\vec{\rho}_s$ rotates $\vec{v}_s$ away from $\vec{j}_0$.) Observation of such behavior would confirm the basic theoretical picture; in that case, the lack of numerical agreement for v_c in parallel field and flow would presumably have some less basic origin.

(3) It would be valuable to study the specific dissipative mechanism that appears above threshold. If the vectors $\hat{l}$ and $\hat{d}$ undergo some precessional motion, then it might be detectable through the anisotropic attenuation of zero sound.[25] Controlled experiments with well-defined flow rates would be desirable, both for $\chi = 0$ and for finite χ. Another possible way to study the motion of $\hat{l}$ is through NMR,[5,6] but the resulting data are likely to present difficulties in interpretation. Theoretically, it is feasible to predict the NMR for a given texture, but the inverse problem of determining the texture is much less tractable.

An additional aspect of the present calculation is the development of a general nonlinear formalism for the hydrodynamics of an arbitrary system described by a free energy. In several cases of interest, the resulting nonlinear equation for the growth of the unstable modes beyond threshold allows a clear decision whether the transition occurs smoothly to a new nearby static texture or catastrophically to some other, qualitatively different (and perhaps time-dependent) configuration. The latter behavior is that predicted here for small χ once the current exceeds the critical value, but the situation might be different for larger χ of order 1. Experiments could help answer this intriguing question.

ACKNOWLEDGMENTS

I am grateful to B. A. Huberman for valuable discussions and for giving me a preliminary draft of Ref. 19. This research was supported in part by the National Science Foundation through Grant No. DMR 78-25258.

[1] Y. R. Lin-Liu, D. Vollhardt, and K. Maki, Phys. Rev. B 20, 159 (1979).

[2] A. L. Fetter and M. R. Williams, Phys. Rev. Lett. 43, 1601 (1979); Phys. Rev. B 23, 2186 (1981).

[3] H. Kleinert, Phys. Lett. 71A, 66 (1979).

[4] See, however, D. Vollhardt and K. Maki, Phys. Rev. B 20, 963 (1979).

[5] M. A. Paalanen and D. D. Osheroff, Phys. Rev. Lett. 45, 362 (1980).

[6] E. B. Flint, R. M. Mueller, and E. D. Adams, J. Low Temp. Phys. 33, 43 (1978).

[7] E. M. Lifshitz and L. P. Pitaevskii, *Statistical Physics*, 3rd ed. (Pergamon, Oxford, 1980), Part 1, Chap. XIV.

[8] W. F. Brinkman and M. C. Cross, in *Progress in Low Temperature Physics*, edited by D. J. Brewer (North-Holland, Amsterdam, 1978), Vol. VIIA, p. 105.

[9] We use dimensionless variables, in which the hydrodynamic parameters are measured in units of $\rho_{\parallel}$, energy density in units of λ_D, length in units of $L^* = (\rho_{\parallel}/\lambda_D)^{1/2} \approx 6$ μm, and H in units of $H^* = (\lambda_D/\lambda_M)^{1/2} \approx 30$ Oe.

[10] This expression differs slightly from that used by R. Kleinberg, J. Low Temp. Phys. 35, 489 (1979). As a result, we reach somewhat different conclusions concerning equilibrium textures.

[11] Since S. Takagi [J. Phys. C 8, 1507 (1975)] has performed essentially the same analysis, we omit the details. Note, however, that our final expressions involve $\vec{j}$ instead of $\vec{v}$.

[12] As noted in Ref. 5, M. C. Cross has independently obtained this value (apart from a factor $\rho_{\parallel}/\rho_0$) for $H \to \infty$ by considering the free energy in an external flow. The same approach works for $\chi \neq 0$.

[13]A. L. Fetter, Phys. Rev. B 20, 303 (1979).
[14]This predicted field dependence is not inconsistent with that seen in Ref. 5, although the observed critical value is smaller by a factor ≈ 0.6.
[15]C. Normand, Y. Pomeau, and M. G. Velarde, Rev. Mod. Phys. 49, 581 (1977).
[16]D. D. Joseph, *Stability of Fluid Motions* (Springer-Verlag, Berlin, 1976), Vol. II, Sec. 82.
[17]See, for example, A. L. Fetter and J. D. Walecka, *Theoretical Mechanics of Particles and Continua* (McGraw-Hill, New York, 1980), Sec. 22.
[18]A. C. Newell and J. A. Whitehead, J. Fluid Mech. 38, 279 (1969).
[19]E. Coutsias and B. A. Huberman (unpublished).
[20]M. C. Cross, Phys. Fluids 23, 1727 (1980).
[21]A. L. Fetter, in *Recent Progress in Many-Body Theories,* edited by J. W. Clark, M. Fortes, M. de Llano, and J. G. Zabolitsky (Springer-Verlag, Berlin, in press).
[22]This step assumes that $\Omega^{(i)}(\epsilon\vec{w})$ tends uniformly to $\Omega^{(i)}(\vec{0})$ as $\epsilon \to 0$. In fact, the present problem is slightly more intricate because $A(\vec{k})$ and $C(\vec{k})$ approach limits that depend on the direction of $\hat{k}$, but this subtlety is irrevelant here.
[23]M. Bagley, P. C. Main, J. R. Hook, D. J. Sandiford, and H. E. Hall, J. Phys. (Paris) 39, Colloq. C6-13 (1978).
[24]A. J. Dahm, D. S. Betts, D. F. Brewer, J. Hutchins, J. Saunders, and W. S. Truscott, Phys. Rev. Lett. 45, 1411 (1980).
[25]D. N. Paulson, M. Krusius, and J. C. Wheatley, Phys. Rev. Lett. 37, 599 (1976).